Progress in Organic Coatings 77 (2014) 247–256

Contents lists available at ScienceDirect

Progress in Organic Coatings

journal homepage: www.elsevier.com/locate/porgcoat

Furan resins as replacement of phenolic protective coatings: Structural, mechanical and functional characterization

G. Rivero[a], L.A. Fasce[b], S.M. Ceré[c], L.B. Manfredi[a,*]

[a] Ecomateriales – Instituto de Investigaciones en Ciencia y Tecnología de Materiales (INTEMA), Universidad Nacional de Mar del Plata, Juan B. Justo 4302, 7600 Mar del Plata, Argentina
[b] Ciencia e Ingeniería de Polímeros – Instituto de Investigaciones en Ciencia y Tecnología de Materiales (INTEMA), Universidad Nacional de Mar del Plata, Juan B. Justo 4302, 7600 Mar del Plata, Argentina
[c] Electroquímica y Corrosión – Instituto de Investigaciones en Ciencia y Tecnología de Materiales (INTEMA), Universidad Nacional de Mar del Plata, Juan B. Justo 4302, 7600 Mar del Plata, Argentina

ARTICLE INFO

Article history:
Received 5 June 2012
Received in revised form 29 April 2013
Accepted 27 September 2013
Available online 27 October 2013

Keywords:
Furan resins
Phenolic resins
Organic protective coatings
Nanoindentation

ABSTRACT

Phenolic coatings are usually a convenient and economical way to protect metallic materials against wear and corrosion. Furan resins are analogous to phenolics, as they are obtained by replacing formaldehyde by furfural in their formulation. In this work, a furan resin based on furfural and phenol was synthesized and used as an aluminum coating. Thus, toxic emissions of formaldehyde were avoided, while a biobased derivative was used instead. The performance of the proposed resin was compared with the one of a traditional phenolic resin. Physicochemical characteristics including chemical structure, surface polarity and glass transition temperature were evaluated by means of Fourier transform infrared spectroscopy, contact angle measurements and dynamic–mechanical analysis, respectively. Nanomechanical and nanotribological properties were assessed by depth sensing indentation techniques. As well, the corrosion resistance of the furan coating was determined by potentiodynamic polarization tests. The obtained results validate the furan resin as a feasible alternative to phenolics to protect aluminum.

1. Introduction

Phenolic resins, synthesized from phenol and formaldehyde, have excellent chemical and thermal resistance, compatibility and reactivity with other resins. Due to these desirable properties, they have been widely used for over 100 years in many industrial applications that range from molding compounds to laminates, adhesives and protective coatings [1–3]. Particularly, the latter application takes advantage of their minimal thermal expansion together with their high resistance to abrasion, wear and corrosion. For example, they are used as protective interior varnishes, electrical insulators layers and anticorrosion coatings for metals, thus preventing the direct contact of metallic substrates with the medium [4,5]. However, due to its high toxicity, there are rigorous regulations concerning the reduction of formaldehyde emissions since the 80s [6–13]. The main restriction is pointed to indoor applications, but formaldehyde release can also occurs in every production, usage, storage, transportation and deposition stage of products containing residual formaldehyde [7].

Following the current tendencies to a minimization of petroleum-based materials, furfural is an appealing option to replace formaldehyde in the resins formulation. Furfural can be easily obtained from agriculture wastes; it is harmless to the ozone layer and is not as toxic as formaldehyde is. Novolak resins prepared from furfural, phenol and formaldehyde have been used during decades for molding compounds, and many commercial patents have been registered [14–17]. Despite the great efforts to eliminate formaldehyde from formulations, up to our knowledge, there is only one recent commercial register for molding resins based on furfuryl alcohol, glyoxal and urea, without formaldehyde [18].

The reaction between phenol and furfural to give a furan resin without using formaldehyde in the initial formulation has been recently studied in our group [19,20]. In this work, the formulated furan resin was proposed as a potential protective coating for aluminum in replacement of the traditional phenolic resins. The anticorrosion function of the coating may be strongly related to its mechanical performance, thus directly influenced by its chemical structure. Hence, an extensive experimental analysis was carried out to evaluate the efficiency of the proposed coating.

In order to characterize the mechanical performance of thin coatings deposited onto substrates, nanoindentation combined with nanoscratch tests appear as the most appropriate and accurate techniques [21–24]. In a nanoindentation test, a tip of well-defined

* Corresponding author. Tel.: +54 223 4816600; fax: +54 0223 4810046.
E-mail addresses: grivero@fi.mdp.edu.ar (G. Rivero), lfasce@fi.mdp.edu.ar (L.A. Fasce), lbmanfre@fi.mdp.edu.ar (L.B. Manfredi).

0300-9440/$ – see front matter © 2013 Elsevier B.V. All rights reserved.
http://dx.doi.org/10.1016/j.porgcoat.2013.09.015

geometry is driven into the material surface while the applied force and tip displacement data are collected. From nanoindentation data, near surface elastic and plastic properties can be easily determined using the widespread method of analysis proposed by Oliver and Pharr [25]. This method has been already applied to characterize different polymeric films with success [26,27] but requires suitably designed experiments. In a nanoscracth test, the tip is moved over the surface while a constant or progressive normal load is applied. The tangential force and the normal displacement are recorded. Nanoscratch tests have been effectively used to determine the friction coefficient and scratch resistance of polymeric coatings and to study the near surface deformation mechanisms [28]. In addition, the adhesion strength can be evaluated for coating/substrate systems, provided that coating debonding along the interface occurs in response to load [26,29].

The corrosion protective quality of coatings can be characterized by potentiodynamic polarization tests that measure the current density generated after applying a cyclic potential to the coated metal sample. An electrical response implies the existence of pores or defects that allow the passage of ions, thus evidencing certain corrosion damage. This technique has been successfully employed to evaluate the corrosion process of several metal/polymer coating systems [30–33].

In this work, a deep study concerning the comparison of physicochemical characteristics and surface nanomechanical behavior of furan and phenolic resins deposited onto aluminum was carried out. In addition, the corrosive protection of the furan coating to aluminum was evaluated.

2. Experimental

2.1. Materials and sample preparation

A resol-type phenolic prepolymer was prepared with a formaldehyde to phenol molar ratio equal to 1.3. Samples of phenol and a formaldehyde aqueous solution (37%, wt/wt) (Cicarelli) were placed in a stainless steel reactor equipped with a low velocity stirrer, a thermometer and a reflux condenser. The pH was kept at 9.0 with a solution of NaOH 40% (wt/wt) and the mixture was allowed to react for 2 h at 90 °C. Thereafter, the mixture was neutralized with a solution of boric acid until a pH value of 6.8–7.0 was reached. A 10 wt% solution of phenolic prepolymer in acetone was prepared.

A furan prepolymer was synthesized from phenol (Anedra) and furfural (Fluka). Phenol was molten into a reactor supplied with a refrigerant, a thermometer and constant mechanical stirring. The reaction media was adjusted using an aqueous solution of K_2CO_3 40 wt/vol%. After heating up to 135 °C, furfural was dropped during 30 min in a furfural to phenol molar ratio equal to 1. The temperature was maintained at 135 °C for 4 h. A detailed chemical and structural characterization of the furan prepolymer has been previously reported [20]. The furan prepolymer was then heated up to 110 °C and 12 wt% of hexamethylenetetramine (HMTA) was added as a catalyst. A 10 wt% solution of furan prepolymer in acetone was prepared.

Different samples of aluminum (6063-TG) coated with both types of resins were made. The aluminum substrate was previously polished with increasing grades of silicon carbide paper and alumina suspensions with particle sizes up to 0.05 μm. Polymeric films of different thickness were prepared by dip-coating process using the prepolymer solutions and two different withdrawal rates (50 and 100 cm/min). In all cases, the immersion time was 4 s.

A two-step thermal curing cycle was applied to both types of coated aluminum plates. They were first heated from room temperature to 120 °C at 1 °C/min and the samples were kept for 30 min at this temperature to allow the release of water and oligomer bubbles. In the second step, the temperature was raised up to 180 °C (for furan coatings) and 190 °C (for phenolic coatings) at 1 °C/min and kept for 30 min to complete the curing.

Hereafter coated aluminum samples are identified as F-50 and F-100 for furan coatings and P-50 and P-100 for phenolic coatings. The numbers indicate the dipping withdrawal rate.

2.2. Methods

2.2.1. Viscosity measurements

The viscosity of the 10 wt% prepolymer solutions was measured in an Anton Paar Physica Rheometer (MCR 301-CC27) at 20 °C, with a configuration of concentric cones. The stationary viscosity was measured among 1 and 100 rpm using 20 ml of solution sample.

2.2.2. Fourier transform infrared analysis (FTIR)

The evolution of characteristic bands associated to different functional groups was followed by FTIR analysis through the whole curing cycle. Spectra were obtained in a Mattson Genesis II, transmission mode, equipped with a heating furnace. Samples were scanned every 10 °C from room temperature to 180 °C in the range of 600–4000 cm^{-1}. For comparison purposes, spectra were normalized with the intensity of the band assigned to the C=C benzene ring stretching (1595 cm^{-1}) whose value is expected to remain constant [34].

2.2.3. Dynamic mechanical analysis (DMA)

DMA experiments were carried out in a Perkin Elmer DMA 7 at a heating rate of 10 °C/min from 15 to 300 °C and at a frequency of 1 Hz. Prismatic specimens were cut from plaques obtained by curing the resins between two glass slides previously treated with silicon release agent (Siliar S.A., Argentina).

The glass transition temperature (T_g) was taken as the temperature corresponding to the maximum displayed in the tan δ curve. The average results of three replicas were reported.

2.2.4. Contact angle measurements

Static contact angle determination was made by the sessile drop method using a Ramé Hart model 500 Advanced Contact Angle Goniometer/Tensiometer equipped with DROPimage Advanced Software. Drops of 5 μl of doubly distilled water were placed onto the surfaces of coated samples. The average contact angle of six drops was reported for each coating.

2.2.5. Scanning electronic microscopy (SEM) and Calotest®

SEM and Calotest experiments were used to determine the actual thickness of furan and phenolic coatings.

SEM was performed in a JEOL JSM-6460LV equipment. Samples were cryofractured and coated with a 300 Å gold layer previously to expose their lateral side. A typical micrograph is shown in Fig. 1.

Coated samples were ground by a rotating steel ball of 30 mm diameter in a Calotest Compact unit from CSM Instruments. It was operated at 2500 rpm for 2 min with an abrasive suspension (0.2 μm particles). Coating thickness was determined by optical inspection of the abraded coating and substrate section applying a geometrical relationship [35].

2.2.6. Nanoindentation and nanoscratch tests

Nanoindentation and nanoscratch experiments were carried out on coated samples in a Triboindenter Hysitron equipped with a Scanning Probe Microscope module (SPM).

Analysis procedures for determining reliable mechanical properties of thin polymeric films deposited onto metal substrates by nanoindentation are not yet standardized as for other engineering materials. For the sake of simplicity and aiming to compare

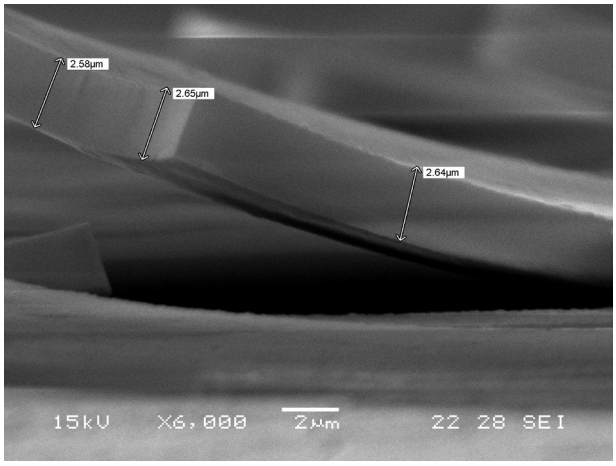

Fig. 1. Coating thickness determination by SEM analysis in F-100 sample.

nanomechanical properties of furan and phenolic films, experiments were accurately designed to apply the simple Oliver and Pharr approach [25,36].

Nanoindentation tests were performed under load control conditions using a diamond Berkovich tip. Maximum loads (P_{max}) were varied from 0.1 to 9 mN to obtain properties at different indentation depths aiming to analyze the possible influence of the aluminum substrate [37,38].

For each loading condition, 5 indentations were made. A holding period of 15 s was applied at maximum load between loading and unloading stages to minimize the creep effect on the unloading curve [39,40]. Tip displacement was corrected by thermal drift using the standard Hysitron routine.

Using the approach outlined by Oliver and Pharr, reduced elastic modulus (E_r) and indentation hardness (H) were calculated as a function of indentation depth [25,36]. As well, the maximum load to contact stiffness-squared parameter (P/S^2), which is a measure of the material resistance to permanent deformation, was evaluated [27,41]. The contact stiffness (S) was calculated from the initial slope of the unloading curve.

Two types of nanoscratch experiments were performed. In the first one, a diamond Berkovich tip was used to obtain the friction coefficient. A constant load of 100 µN, a sliding speed of 0.33 µm/s, and a lateral displacement of 10 µm were applied. For each sample, 10 experiments were carried out. The apparent friction coefficient (μ) was calculated as the ratio of the measured tangential (F_x) and normal (F_z) forces. The second type was intended to analyze the surface damage behavior during scratch deformation of furan coatings. A diamond spherical tip with 2 µm radius of curvature was slid at a speed of 0.33 µm/s while the load was linearly increased up to 9 mN, which was the maximum force experimentally available.

2.2.7. Potentiodynamic polarization

Potentiodynamic polarization tests were carried out with a standard three-electrode system to quantify the anticorrosive protection of the furan coating. The specimens were connected to the aluminum either coated or uncoated as working electrode, a pure platinum wire was used as the counter electrode and standard calomel electrode (SCE) was used as the reference electrode. Potentiodynamic scans were performed in NaCl solution (0.15 mol/L) from −0.8 to 0.5 V at a scan rate of 1 mV/s and backwards. The polarization curves were measured in a Gamry Ref 600 electrochemical unit (Gamry Instrument, USA) initially and, after 12 and 30 days of immersion in the solution at 20 °C.

3. Results and discussion

3.1. Physicochemical characterization

The synthesis of phenolic resins starts with the addition of formaldehyde to the phenol *ortho* and *para* positions. Then, condensation reactions take place during curing in which methylene bridges are formed and water and formaldehyde are released, as schematized in Fig. 2.

Characteristic infrared spectra wavelengths corresponding to substituted benzene rings as well as methylene bridges in the chemical structure of phenolic resins are well documented [42–44]. The bands corresponding to methylene bridges, directly related to the crosslinking density, appear in the 1400–1500 cm^{-1} wavelength range of the infrared spectra, and their specific position

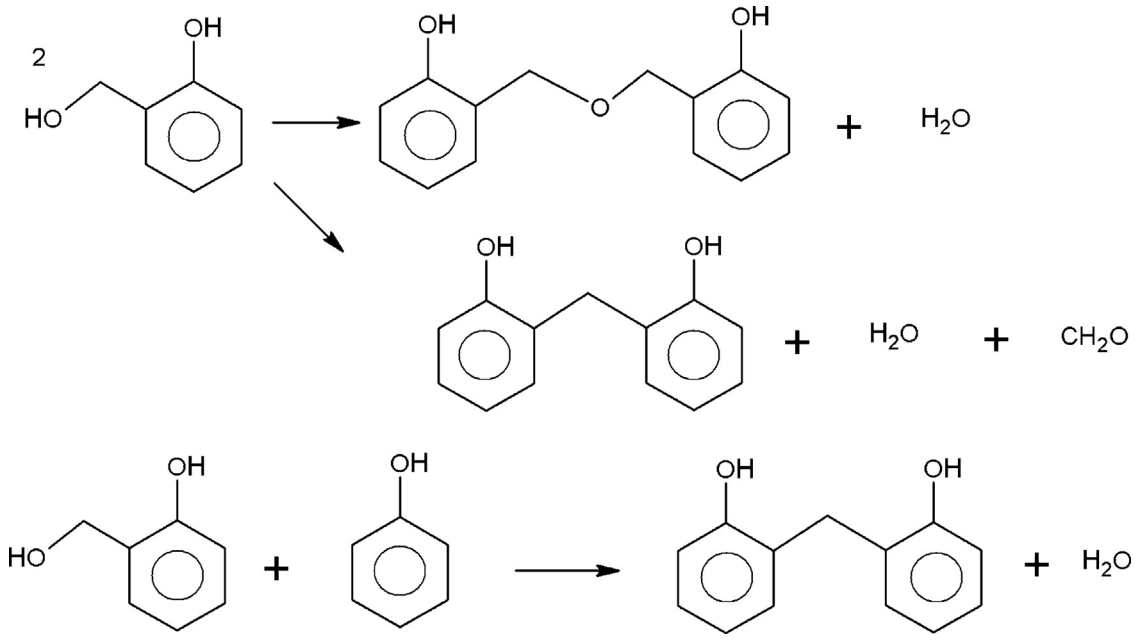

Fig. 2. Scheme showing the condensation reactions that take place during curing of phenolic resins.

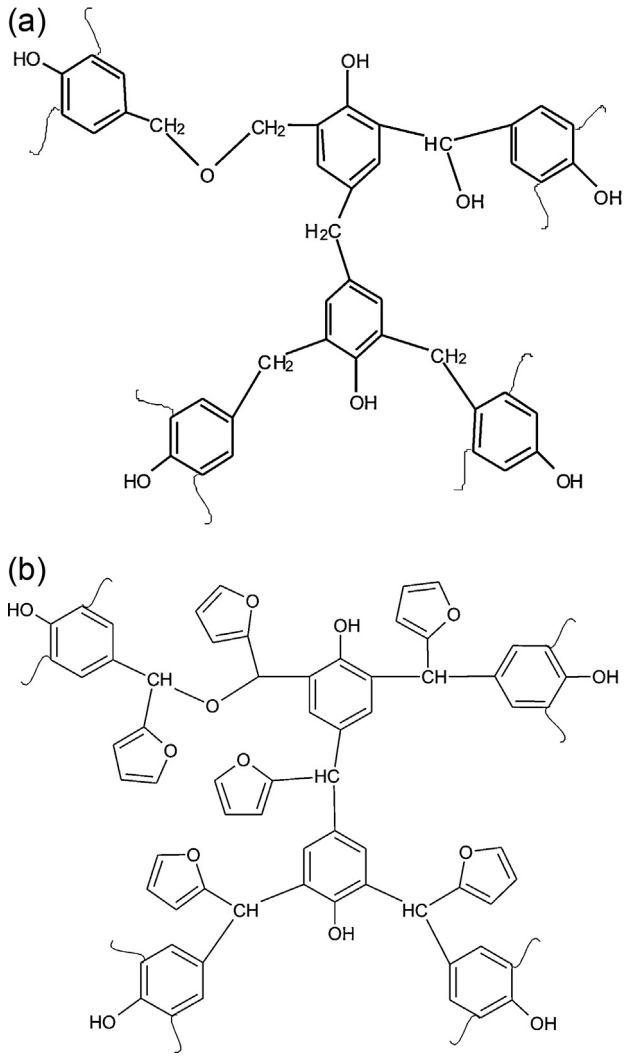

Fig. 3. Scheme showing the chemical structure of (a) phenolic and (b) furan resins.

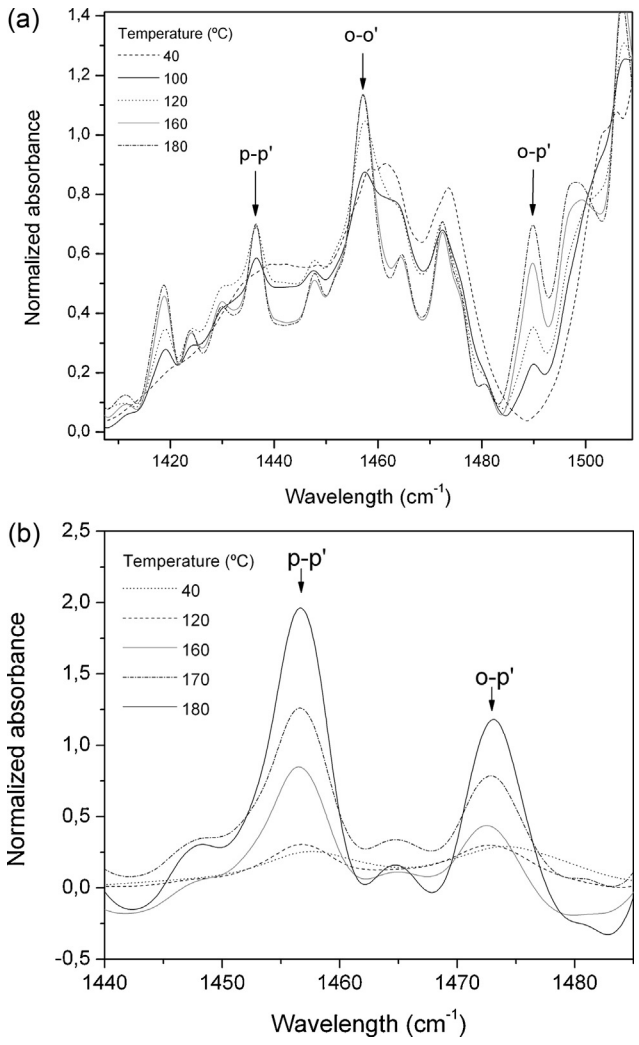

Fig. 4. Region of the FTIR spectra showing the characteristic bands corresponding to bridges in (a) furan and (b) phenolic resin. Some spectra obtained at different temperatures during curing are shown.

can be related to a particular position in the phenol ring; *i.e. para–para′* (*p–p′*), *ortho–ortho′* (*o–o′*) and *ortho–para′* (*o–p′*) methylene bridges, respectively [34]. Similarly, —CH— bridges are formed in furan resins during their curing reactions. The resulting highly crosslinked structure of both resins are shown in Fig. 3 [4,45].

As expected, furan and phenolic resins displayed similar FTIR spectra due to their analogous chemical structure though slight differences were observed. The three types of bridges were assigned in the furan resin spectra (Fig. 4a), but the band associated with *o–o′* bridges was not detected in the phenolic resin spectra (Fig. 4b) consistently with previous reports [46,47]. The variation in the amount of bridges formed during curing is compared in Fig. 5. The amount of *o–p′* and *p–p′* bridges was larger in the completely cured phenolic resin, but additional *o–o′* bridges appeared in the furan one. However, the final amount of total bridges contained in both resins resulted similar.

The values of glass transition temperature (T_g) and storage modulus in the rubbery state (E'_{rubber}) of phenolic and furan resins arisen from DMA experiments are reported in Table 1. T_g and modulus values of both resins were practically identical, evidencing their similar chemical structure. Moreover, as E'_{rubber} is directly related to crosslink density [48], the total amount of bridges appeared to be very similar in both resins in agreement with FTIR results (Fig. 5).

The contact angle measurements for both types of coated samples are included in Table 1. The lower value measured for the furan

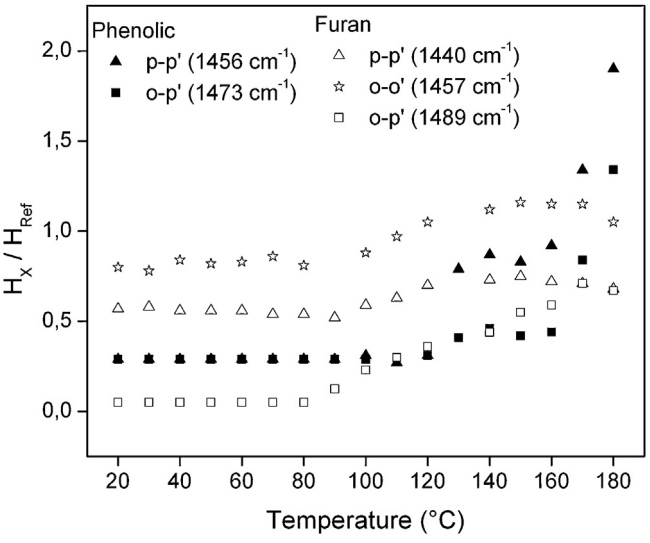

Fig. 5. Evolution of the bridges amount in phenolic and furan resins during curing.

Table 1
Dynamic-mechanical properties and contact angle of the resins.

Resin	E'_{rubber} (GPa)	T_g (°C)	Contact angle (degree)
Phenolic	0.25	255	74.9 ± 0.8
Furan	0.24	252	66.8 ± 2.5

Table 2
Coating thickness values of furan and phenolic samples.

Sample	P-50	P-100	F-50	F-100
Coating thickness (μm)	0.24 ± 0.08	0.29 ± 0.08	2.14 ± 0.10	2.62 ± 0.04

coating displayed its greater hydrophilic character. The higher polarity is a result of the polar groups in the furan coating surface, but it is also related with the interaction between these groups and the hydroxyls of the aluminum substrate, as it will be later discussed.

3.2. Coating thickness

Actual thickness values of furan and phenolic coatings measured by SEM and verified by Calotest® experiments are reported in Table 2. Phenolic films were notably thinner than furan ones when prepared using the same prepolymer solution concentration and withdrawal rate. As expected, the coating thickness decreased as the withdrawal rate diminished for each type of resin.

It is well known that the dip coating process is controlled by several forces such as gravitational, inertia, capillary and viscous drag [49,50]. The latter force moves the liquid solution upward with the substrate and it is proportional to the liquid viscosity and withdrawal speed. So, larger solution viscosities and withdrawal speeds lead to thicker coatings.

The viscosities of the 10% (w/w) solutions of furan and phenolic prepolymers in acetone were 17.93 ± 0.24 cP and 3.95 ± 0.12 cP, respectively. So, the great difference in the resulting coating thicknesses can be directly related to the dissimilar viscosity of their prepolymer solutions.

The withdrawal speed, u_0, is the most common parameter used to control the film thickness, t. The relationship between t and u_0 is usually expressed as a power law mathematical form ($t \propto u_0^x$) with x values ranging from 0 to 1 [51]. Fig. 6 shows thickness data plotted according to the mentioned correlation. For both coatings a value of x about 0.3 was observed, evidencing the same thickness dependence with withdrawal speed. Hence, as differences in thickness are mainly due to the viscosity, similar values for both coatings could be achieved by adjusting the solution concentration.

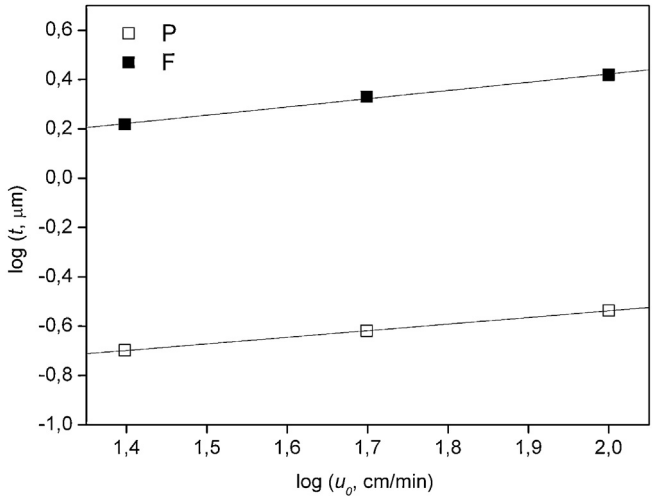

Fig. 6. Relationship between coating thickness and withdrawal rate for phenolic and furan resins. Additional data at 25 cm/min are also included.

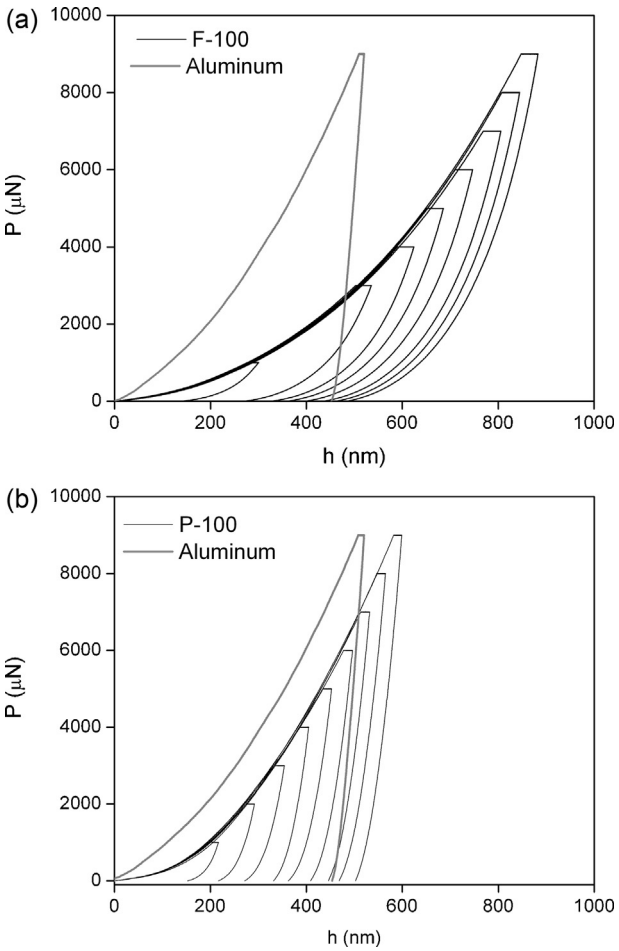

Fig. 7. Load *vs.* indentation depth curves for different maximum applied loads for (a) F-100 and (b) P-100 systems. The indentation response of the aluminum substrate is included for comparison.

3.3. Nanomechanical properties

Typical load–depth curves obtained at different maximum applied loads for two of the studied systems are shown together with the substrate response in Fig. 7. The mechanical response of the coated systems was completely different from the one of the substrate. While aluminum deformed plastically, the coating was able to elastically recover deformation after the tip was removed from the surface. Properties were determined as a function of indentation depth and analyzed considering the influence of the underlying substrate. The time-dependence of the indentation response of the systems was clearly evident by the increase in indentation depth during the holding period at peak load (indentation creep). For the thickest coatings (*i.e.* F-100 in Fig. 7a), loading curves practically overlapped while the shape of unloading curves changed with increasing maximum applied load. For the thinner coatings (*i.e.* P-100 in Fig. 7b), the curves resembled the aluminum response especially at high indentation loads. For all cases, load–depth curves did not exhibit discontinuities, which are generally attributed to failure events like coating detachment [52–54]. Therefore, the adhesion of both furan and phenolic films to the aluminum substrate appeared to be very good.

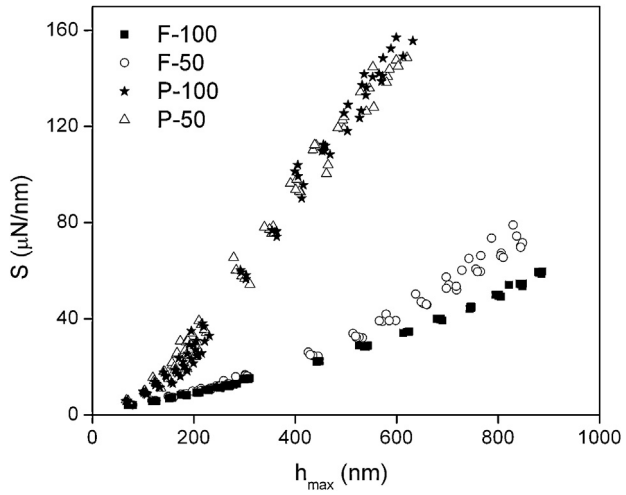

Fig. 8. Contact stiffness *vs.* indentation depth for furan coatings and phenolic coatings on aluminum.

The contact stiffness values, S, are plotted against maximum penetration depth in Fig. 8. For a homogeneous material, S is expected to increase linearly with indentation depth since elastic modulus does not vary with depth [38]. Data showed a positive deviation from linearity, which increased with increasing indentation depth or reducing coating thickness. This means that the measured indentation response was influenced by the stiff aluminum substrate.

Reduced elastic modulus values, E_r, obtained from nanoindentation experiments are shown in Fig. 9 as a function of thickness-normalized depth. A value of 72.5 ± 2.8 GPa was independently determined for the aluminum substrate. As expected, the E_r values of the coating/substrate systems increased with indentation depth. These values represent an apparent property which combines the mechanical properties of the coating and the underlying substrate, and are not an elastic modulus profile through the coating [22]. The dissimilar h_{max}/t range achieved in the experiments for furan and phenolic coatings was due to the large difference in their thicknesses (Table 2).

For furan coatings, a plateau value was clearly observed at very low indentation depths (Fig. 9a). This value was the intrinsic elastic modulus of the furan coating. It coincided with the value determined by applying the "10% rule", which establishes that for compliant coating/stiff substrate systems and for coatings thicker than 1 μm, the elastic modulus of the coating can be evaluated at depths lower than 1/10 of the coating thickness [25,55]. The E_r values of furan coatings turned out to be independent on coating thickness and near 10 GPa (Table 3).

On the contrary, a plateau value could not be observed for the case of phenolic coatings (Fig. 9b). Because coatings were too thin (about 0.2 μm), the minimum experimentally achievable h_{max}/t range resulted higher than 1/10 of the coating thickness. Obtaining reliable indentation curves at very low displacements (<20 nm) is generally difficult since uncertainties appear due to errors in contact area estimations, surface roughness, tip variations and signal vibrations. In this case, to extract the intrinsic elastic modulus of phenolic coatings, a model proposed in the literature for compliant coating/stiff substrate systems was applied [56,57]. The model considers the contribution of coating and substrate modulus to the apparent modulus as a function of contact depth, h_c [56], as:

$$E^* = E_c + (E_s - E_c) \times e^{-(\alpha \times t/h_c)} \quad (1)$$

where E^* represents the apparent reduced elastic modulus, E_c and E_s are the intrinsic properties of the coating and the substrate, t is the actual coating thickness and α is a fitting parameter. If E_s is known, the model fitting provides the values of E_c and α. The mathematical form of Eq. (1) predicts a plateau value for low contact depths. Fitted model parameters are shown in Table 3. The α parameter increased while decreasing the coating thickness indicating a not straightforward dependence of apparent modulus with coating thickness, which is associated with the complex stress field. The E_c value of the phenolic coating was very similar to the one of the furan coating. Note that, this model also described quite well the furan systems behavior (Fig. 10 and Table 3). The E_c value of furan coatings coincided with the modulus obtained by the "10% rule".

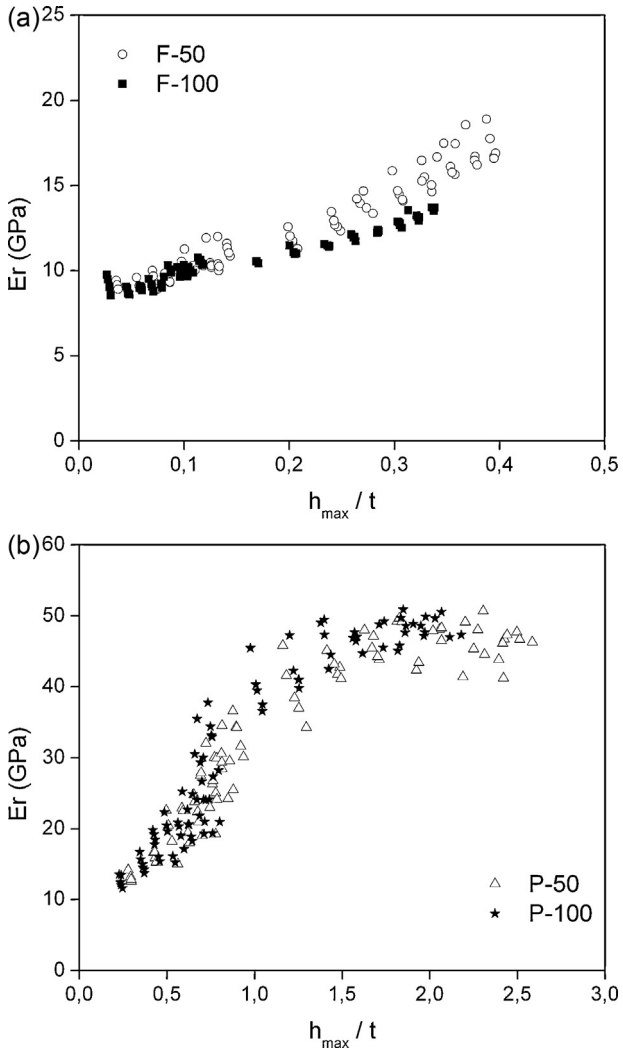

Fig. 9. Reduced elastic modulus values as a function of thickness normalized indentation depth for (a) furan coatings and (b) phenolic coatings deposited onto aluminum substrate.

Indentation hardness values, H, plotted as a function of thickness-normalized depth for furan and phenolic systems (Fig. 11) exhibited a completely different behavior than E_r values. For each type of coating, H data belonging to different thicknesses overlapped. This can be attributed to the less spatially spread plastic strain field beneath the indenter in comparison to the elastic strain field. As a consequence, for a given indentation depth, the substrate influence on hardness resulted lower than on indentation modulus [58].

An almost constant H value was observed for furan coatings (Fig. 11a) in the whole indentation range; *i.e.* up to h/t equal to 0.4. The averages of H values were taken as the intrinsic coating

Table 3
Intrinsic nanomechanical properties of furan and phenolic films.

Property	Method	F-50	F-100	P-50	P-100
Coating elastic modulus (GPa)	"10% rule"	9.8 ± 0.7	9.5 ± 0.6	–	–
	(E_c) Eq. (1)	10.2 ± 0.1 (R^2 = 0.91)	9.7 ± 0.1 (R^2 = 0.87)	12.4 ± 1.2 (R^2 = 0.93)	10.5 ± 1.2 (R^2 = 0.92)
Coating hardness (GPa)	Average value	0.63 ± 0.03	0.62 ± 0.05	–	–
	(H_c) Eq. (2)	–	–	0.57 ± 0.04 (R^2 = 0.82)	0.59 ± 0.02 (R^2 = 0.89)

hardness (Table 3). The intrinsic hardness of the furan coating was about a half of the aluminum hardness.

On the other hand, H values increased with increasing thickness-normalized depth for the case of phenolic coatings (Fig. 11b). Moreover, it is observed that for h_{max}/t larger than 1, H data approached the value of the aluminum (1.15 ± 0.05 GPa). Aiming to obtain the intrinsic hardness of phenolic coatings, a simple model proposed by Bhattacharya and Nix [59] was applied. The model considers the combined effect of substrate and coating properties on the apparent hardness as a function of indentation depth, as:

$$H* = H_s + (H_c - H_s) \cdot \exp\left(-\alpha_n \cdot \left(\frac{h}{t}\right)^n\right) \quad (2)$$

where H^* represents the apparent hardness, H_c and H_s are the intrinsic properties of coating and substrate, β is a fitting parameter and n is equal to 2 for the case of soft coatings/hard substrates systems [23]. The fitted H_c values are reported in Table 3. The H_c value of the phenolic coating was very close to the H value displayed by the furan coatings.

The values of the ratio of maximum load to stiffness squared, P_{max}/S^2, *i.e.* the material's resistance to plastic deformation [54], are plotted as a function of thickness-normalized depth in Fig. 12 for both types of coatings. Due to the influence of the substrate, P_{max}/S^2 parameter decreased as the indentation depth increased. However, it clearly emerged that furan and phenolic coatings resulted more resistant to plastic deformation than aluminum substrate. This result could be explained by the beneficial combination of elastic and plastic properties of polymeric coatings in relation to aluminum. Polymeric coatings showed about a 7-fold lower modulus but only 2-fold lower hardness than the substrate. Hence, at a given indentation depth, the coating was able to accommodate a larger amount of elastic deformation than the substrate, leading to a lower permanent damage. In addition, P_{max}/S^2 values of both types of coatings overlapped for the lowest h_{max}/t range, indicating that the mechanical protection conferred by both coatings was similar. Consistently, the H/E_r^2 ratio which is proportional to the P_{max}/S^2 parameter, was almost identical for both types of coatings (Table 3).

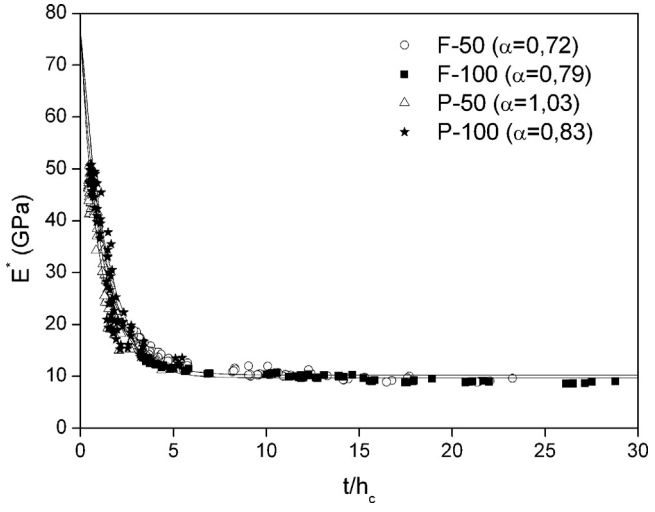

Fig. 10. Reduced elastic modulus as a function of thickness to contact depth ratio. Solid lines show model fittings according to Eq. (1). The α parameter is reported.

3.4. Nanoscratch behavior

The average values of the apparent friction coefficient, μ_{app}, measured at low loads were 0.35 and 0.38 for furan and phenolic coatings, respectively. In these experiments, the scratch grooves were imperceptible indicating that deformation was completely recovered after load removal, *i.e.* an elastic deformation mode prevailed. The μ_{app} values reflected the adhesion characteristics between the coating and the diamond tip since the principal friction mechanism under elastic contact conditions is adhesion. The

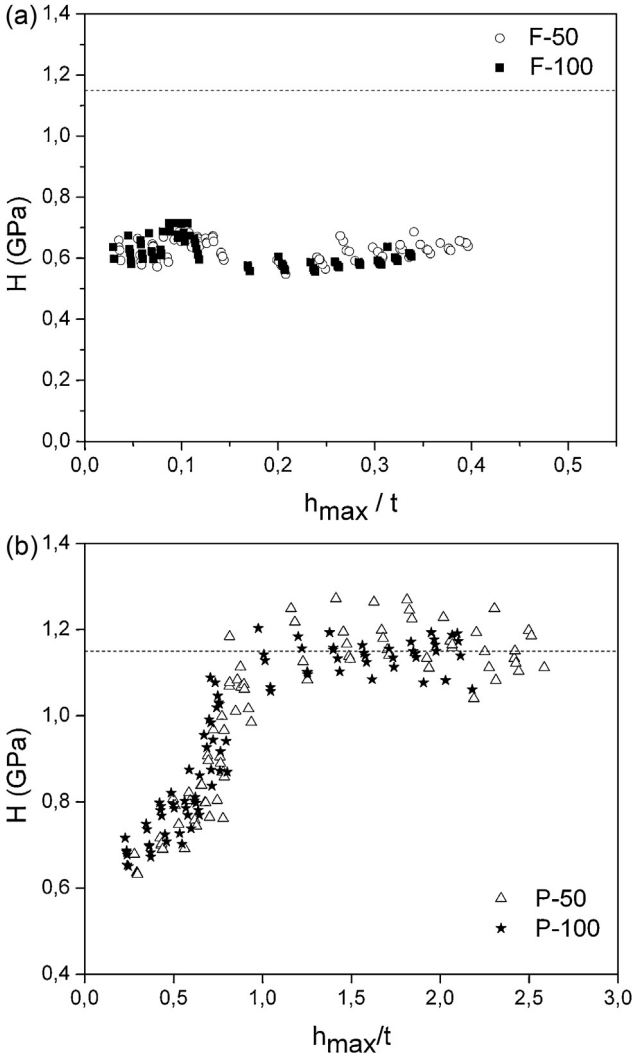

Fig. 11. Hardness values as a function of thickness normalized indentation depth for (a) furan coatings and (b) phenolic coatings deposited onto aluminum substrate. The dashed line represents the hardness of the aluminum substrate.

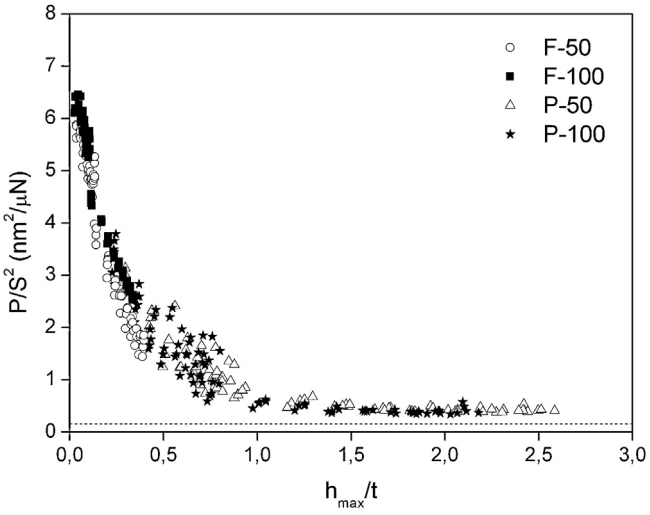

Fig. 12. Maximum load to the stiffness squared values as a function of thickness normalized indentation depth for furan and phenolic coatings. The dashed line represents the value determined for the aluminum substrate alone.

slightly lower μ_{app} of the furan resin was consistent with its higher polarity.

The damage mechanism was investigated through nanoscratch experiments under increasing normal load. A typical response obtained for furan coatings is shown in Fig. 13. An almost constant slope in the normal displacement *vs.* lateral displacement curve was observed indicating that the mechanical response was uniform. The apparent friction coefficient increased with increasing the normal force (or scratch distance) consistently with a deformation mechanism of ductile ploughing [60]. SPM images of the scratch grooves revealed that during the sliding process the furan coating deformed plastically and accumulated at both sides of the track as well as ahead of the crack tip (Fig. 14). The scratch process caused shear-dominant stresses in the immediate vicinity of the tip, thus promoting shear yielding of the furan resin [61]. As well, in SPM images there were no evidences of coating delamination, demonstrating that the adhesion strength between furan coating and aluminum was excellent. It is known that for the case of a compliant coating on a stiff substrate, delamination could occur if the shear stress along the interface exceeds the adhesion strength of the system because the shear stress tends to dislocate the

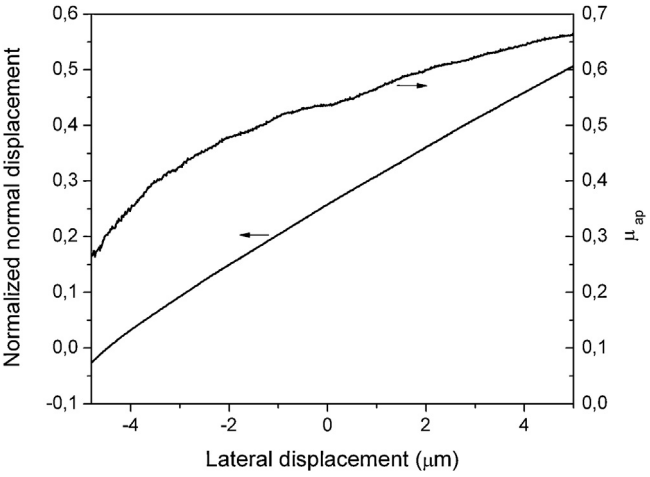

Fig. 13. Normal displacement and friction coefficient as a function of lateral displacement measured for F-100 sample in Nanoscratch tests under ramping normal loading.

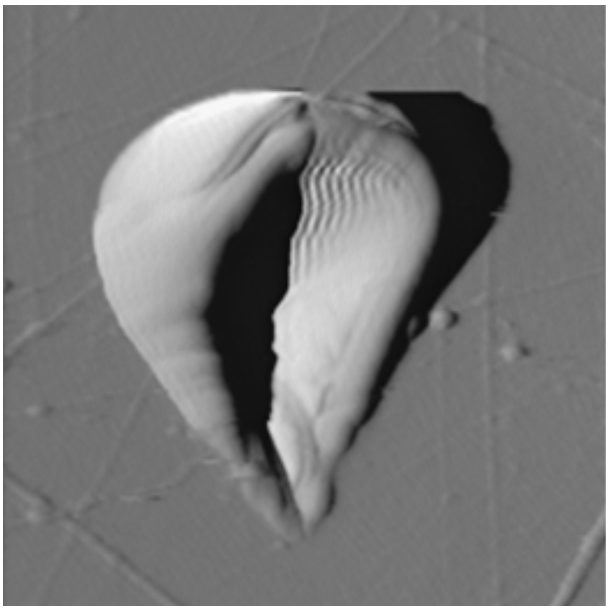

Fig. 14. SPM image of the scratch groove left on the furan coating surface of F-100 sample after ramping normal loading.

coating [62]. A similar scratch behavior was observed for the phenolic coating.

In resume, nanoscratch tests showed that coating deformation mechanism was dominated by the yield stress. As the indentation hardness, which is proportional to the yield stress, of furan and phenolic resins was practically the same, it can be stated that there is no difference in the mechanical protection that both types of coatings offered to the aluminum substrate.

3.5. Corrosion behavior

Results of potentiodynamic polarization tests at different immersion times are shown in Fig. 15 for uncoated and furan coated aluminum specimens.

After immersion in the NaCl solution, the uncoated aluminum showed a strong diminution of the current density in the vicinity of the corrosion potential, due to the development of a passive film that remained stable in the assayed period. The electrochemical response of uncoated and furan coated specimens showed clear differences. For the coated sample, the current density decreased

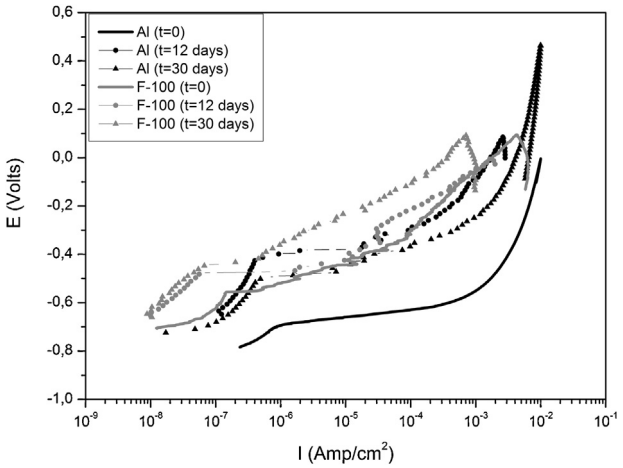

Fig. 15. Typical potentiodynamic polarization curves of uncoated and furan coated aluminum samples.

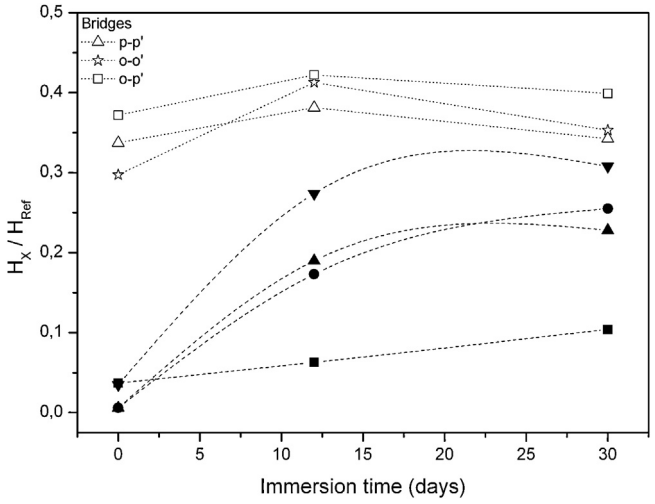

Fig. 16. Change of the relative amount of the bands corresponding to the hydroxylated aluminum species measured at the wavelenghts: (■) 670 (stretch Al—O), (●) 738 (longitudinal stretch Al—O), (▲) 763 (vibrations Al—O) y (▼) 830 cm^{-1} (vibrations Al—OH), with immersion time. Evolution of furan bridges amount during immersion time is also included.

approximately one order of magnitude with respect to the uncoated aluminum. This fact can be attributed to the diminution of the substrate exposed area. However, after a long-time immersion, it followed the same trend as the uncoated material because of the formation of the passive film, and the corrosion protection was improved with the immersion time.

As expected, local corrosion spots were formed after the potentiodynamic destructive tests. Nevertheless, neither delamination nor furan coating detachment was evidenced in the surrounding of such defects.

The good adhesion between the organic furan coating and the aluminum substrate could be attributed to the excellent affinity among the hydrophilic groups of the polymer (Fig. 3) and a hydroxylated aluminum surface. It is well known that when aluminum is in contact with air a thin layer of aluminum oxide is spontaneously formed and then, ambient water is absorbed on that layer causing the hydroxylation of the aluminum oxide surface [63]. The presence of such hydroxylated aluminum species in the coated samples immersed in NaCl solution was verified by FTIR analysis. There was observed an increase in the intensity of the characteristics bands associated with Al—O, Al—OH [63–67] with increasing exposure time as shown in Fig. 16. On the other hand, it was probed that the chemical crosslinks of the furan coating remained unaltered during the whole corrosion test, as demonstrated in Fig. 16.

4. Conclusions

A deep characterization including physico-chemical, mechanical and aluminum corrosion protection was performed aiming to compare the performance of coatings based on a proposed furan polymer and a traditional phenolic resin.

The coating's thickness obtained using the same prepolymer concentration solutions and dipping rates greatly differed due to the large disparity in furan and phenolic solutions viscosities.

Both resins exhibited similar chemical structures and hence practically the same dynamical–mechanical properties (T_g and E''). As well, it was proved that, despite the difference in thickness, their surface nanomechanical elastic (E_c) and plastic properties (H) are equivalent.

The furan resin showed a greater hydrophilic character than the phenolic one, related to its larger content of polar groups. This was reflected in a slight difference in their apparent friction coefficient (μ_{app}).

Both types of coatings showed the same mechanical protection to aluminum. The scratch deformation behavior was dominated by the yield stress of the polymers (ductile ploughing mechanism) with no evidences of coating delamination.

Furan coatings were able to efficiently protect aluminum from corrosion by conferring a stable barrier. In addition, a combining positive effect was displayed under severe conditions, as the intrinsic aluminum passive film may be capable to block eventual pores or defects in the polymeric film.

The lack of signs of coating detachment confirmed the excellent adhesion of the coating with the substrate, probably due to the great affinity between hydrophilic groups of the furan polymer and the oxides/hydroxides evidenced in the aluminum surface.

It was proved that the proposed furan resin could replace the traditional phenolic resin to protect aluminum against scratch and corrosion.

Acknowledgements

Authors gratefully acknowledge the Consejo Nacional de Investigaciones Científicas y Técnicas (PIP0014) and the Agencia Nacional de Promoción Científica y Tecnológica (PICT0682).

References

[1] M. Biedermann, K. Grob, Phenolic resins for can coatings: I. Phenol-based resole analysed by GC–MS, GC × GC, NPLC–GC and SEC, LWT – Food Science and Technology 39 (2006) 633–646.
[2] M. Biedermann, K. Grob, Phenolic resins for can coatings: II. Resoles based on cresol/phenol mixtures or tert. butyl phenol, LWT – Food Science and Technology 39 (2006) 647–659.
[3] H.-J. Song, Z.-Z. Zhang, Study on the tribological and hydrophobic behaviors of phenolic coatings reinforced with PFW, PTFE and FEP, Surface and Coatings Technology 201 (2006) 1037–1044.
[4] A. Gardziella, L. Pilato, A. Knop, Phenolic Resins: Chemistry, Applications, Standardization, Safety and Ecology, Springer-Verlag, Berlin, Heidelberg, 2000.
[5] A. Sturiale, A. Vázquez, A. Cisilino, L.B. Manfredi, Enhancement of the adhesive joint strength of the epoxy–amine system via the addition of a resole-type phenolic resin, International Journal of Adhesion and Adhesives 27 (2007) 156–164.
[6] Formaldehyde Standards for Composite Wood Products, Act VI, Congress of the United States of America, WA, USA, 2010.
[7] Formaldehyde, Concise International Chemical Assessment, World Health Organization (WHO), Geneva, 2002.
[8] Regulation CE No. 3093/94, in: E.C. Commission (Ed.) 2001/58/CE (2001).
[9] D. 2002/95/EC, Restriction of hazardous substances (RoHS), in: European Parliament (2000).
[10] J. Chang, Z. Guo, R. Fortmann, H. Lao, Characterization and reduction of formaldehyde emissions from a low-VOC latex paint, Indoor Air 12 (2002) 10–16.
[11] G.E. Myers, Advances in methods to reduce formaldehyde emission, in: M.P. Hamel (Ed.), Composite Board Products for Furniture and Cabinets: Innovations in Manufacture and Utilization, Forest Products Research Society, New York, USA, 1989, pp. 58–64.
[12] T. Salthammer, S. Mentese, R. Marutzky, Formaldehyde in the indoor environment, Chemical Reviews 110 (2010) 2536–2572.
[13] M. Šmidriaková, J. Sedliacik, J. Matyasovsky, P. Duchovic, Reduction of formaldehyde emission from plywood bonded with modified UF adhesive, Forestry and Wood Technology 76 (2011) 44–48.
[14] X. Jie, Y. Jun, Methd for Preparing Hot Box Furan Resin, 102153719A, International, 2011.
[15] H. Liu, B. Zhang, Preparation Method of Furan Resin for Casting, CN102161741 (A), International, 2011.
[16] Q. Pu, Thermal cracking resistant hard sand, B22C1/22, International, 2011.
[17] M. Toshiki, Y. Akira, J. Takashi, Binding Composition for Foundry Sand, 2011-131236, Japan, 2011.
[18] L.J. Min, Y.J. Han, P.S. Hun, Furan Resin Composition, Furan Resin-Hardener Composition and Foundry Sand Molds of the Same, KR20110049527 (A), Korea, 2011.
[19] G. Rivero, V. Pettarin, A. Vázquez, L.B. Manfredi, Curing kinetics of a furan resin and its nanocomposites, Thermochimica Acta 516 (2011) 79–87.
[20] G. Rivero, A. Vázquez, L.B. Manfredi, Synthesis and characterization of nanocomposites based on a furan resin, Journal of Applied Polymer Science 117 (2010) 1667–1673.
[21] B. Bhushan, X. Li, Nanomechanical characterisation of solid surfaces and thin films, International Materials Reviews 48 (2003) 125–164.

[22] S. Bull, Nanoindentation of coatings: topical review, Journal of Physics D: Applied Physics 38 (2005) 393–413.
[23] J. Malzbender, J.M.J. den Toonder, A.R. Balkenende, G. de With, Measuring mechanical properties of coatings: a methodology applied to nano-particle-filled sol–gel coatings on glass, Materials Science and Engineering R: Reports 36 (2002) 47–103.
[24] W. Shen, J. Sun, Z. Liu, W. Mao, J.D. Nordstrom, P.D. Ziemer, F.N. Jones, Methods for studying the mechanical and tribological properties of hard and soft coatings with a nano-indenter, JCT Research 1 (2004) 117–125.
[25] W.C. Oliver, G.M. Pharr, An improved technique for determining hardness and elastic modulus using load and displacement sensing indentation experiments, Journal of Materials Research 7 (1992) 1562–1584.
[26] R.A. DiFelice, J.G. Dillard, D. Yang, Chemical and nanomechanical properties of plasma-polymerized acetylene on titanium and silicon, International Journal of Adhesion and Adhesives 25 (2005) 342–351.
[27] L.A. Fasce, V. Costamagna, V. Pettarin, M. Strumia, P. Frontini, Mechanical behaviour of surface modified polypropylene films with acrylic acid as grafting agent, Express Polymer Letters 2 (2008) 779–790.
[28] R.R. Thridandapani, A. Mudaliar, Q. Yuan, R.D.K. Misra, Near surface deformation associated with the scratch in polypropylene–clay nanocomposite: a microscopic study, Materials Science and Engineering: A 418 (2006) 292–302.
[29] S. Bull, E. Berasetegui, An overview of the potential of quantitative coating adhesion measurement by scratch testing, Tribology International 39 (2006) 99–114.
[30] V.J. Gelling, M.M. Wiest, D.E. Tallman, G.P. Bierwagen, G.G. Wallace, Electroactive-conducting polymers for corrosion control: 4. Studies of poly(3-octyl pyrrole) and poly(3-octadecyl pyrrole) on aluminum 2024-T3 alloy, Progress in Organic Coatings 43 (2001) 149–157.
[31] J. Ou, J. Wang, J. Zhou, S. Liu, Y. Yu, X. Pang, S. Yang, Construction and study on corrosion protective property of polydopamine-based 3-layer organic coatings on aluminum substrate, Progress in Organic Coatings 68 (2010) 244–247.
[32] S.S. Pathak, A. Sharma, A.S. Khanna, Value addition to waterborne polyurethane resin by silicone modification for developing high performance coating on aluminum alloy, Progress in Organic Coatings 65 (2009) 206–216.
[33] M. Shabani-Nooshabadi, S.M. Ghoreishi, M. Behpour, Direct electrosynthesis of polyaniline–montmorrilonite nanocomposite coatings on aluminum alloy 3004 and their corrosion protection performance, Corrosion Science 53 (2011) 3035–3042.
[34] L.B. Manfredi, O. de la Osa, N. Galego Fernández, A. Vázquez, Structure–properties relationship for resols with different formaldehyde/phenol molar ratio, Polymer 40 (1999) 3867–3875.
[35] SCM-Instruments, Calotest Technical Features, 2004.
[36] ISO14577-1, Metallic Materials – Instrumented Indentation Test for Hardness and Materials Parameter, International Standard, 2002.
[37] E. Le Bourhis, Indentation mechanics and its application to thin film characterization, Vacuum 82 (2008) 1353–1359.
[38] R. Saha, W.D. Nix, Effects of the substrate on the determination of thin film mechanical properties by nanoindentation, Acta Materialia 50 (2002) 23–38.
[39] K. Geng, F. Yang, T. Druffel, E.A. Grulke, Nanoindentation behavior of ultrathin polymeric films, Polymer 46 (2005) 11768–11772.
[40] A.H.W. Ngan, B. Tanga, Viscoelastic effects during unloading in depth-sensing indentation, Journal of Materials Research 17 (2002) 2604–2610.
[41] D.L. Joslin, W.C. Oliver, A new method for analyzing data from continuous depth-sensing microindentation tests, Journal of Materials Research 5 (1990) 123–126.
[42] T. Holopainen, L. Alvila, J. Rainio, T.T. Pakkanen, IR spectroscopy as a quantitative and predictive analysis method of phenol–formaldehyde resol resins, Journal of Applied Polymer Science 69 (1998) 2175–2185.
[43] L.B. Manfredi, M.J.L. Ginés, G.J. Benítez, W.A. Egli, H. Rissone, A. Vázquez, Use of epoxy-phenolic lacquers in food can coatings: characterization of lacquers and cured films, Journal of Applied Polymer Science 95 (2005) 1448–1458.
[44] C. Rockniak, T. Biernacka, M. Skarzynski, Some properties and chemical structure of phenolic resins and their derivatives, Journal of Applied Polymer Science 28 (2003) 531–542.
[45] K.J. Zeitsch, The Chemistry and Technology of Furfural and its Many By-Products, 1st ed., Elsevier Science, Amsterdam, The Netherlands, 2000.
[46] M.-F. Grenier-Loustalot, S. Larroque, D. Grande, P. Grenier, D. Bedel, Phenolic resins: 2. Influence of catalyst type on reaction mechanisms and kinetics, Polymer 37 (1996) 1363–1369.
[47] M.-F. Grenier-Loustalot, S. Larroque, P. Grenier, J.-P. Leca, D. Bedel, Phenolic resins: 1. Mechanisms and kinetics of phenol and of the first polycondensates towards formaldehyde in solution, Polymer 35 (1994) 3046–3054.
[48] J. Pascault, H. Sautereau, R. Williams (Eds.), Thermosetting Polymers, Marcel Dekker, New York, USA, 2002.
[49] L. Landau, B. Levich, Dragging of a liquid by a moving plate, Acta Physicochimica URSS 17 (1942) 42–54.
[50] P. Schunk, A. Hurd, C. Brinker, Free-meniscus coating processes, in: S.F. Kistler, P.M. Schweizer (Eds.), Liquid Film Coating: Scientific Principles and Their Technological Implications, Chapman & Hall, London, UK, 1997, pp. 673–708.
[51] P. Yimsiri, M.R. Mackley, Spin and dip coating of light-emitting polymer solutions: matching experiment with modelling, Chemical Engineering Science 61 (2006) 3496–3505.
[52] S. Etienne-Calas, A. Duri, P. Etienne, Fracture study of organic–inorganic coatings using nanoindentation technique, Journal of Non-Crystalline Solids 344 (2004) 60–65.
[53] J. Malzbender, G. de With, The use of the indentation loading curve to detect fracture of coatings, Surface and Coatings Technology 137 (2001) 72–76.
[54] J. Malzbender, G. de With, The use of the loading curve to assess soft coatings, Surface and Coatings Technology 127 (2000) 265–272.
[55] A.C. Fischer-Cripps, A review of analysis methods for sub-micron indentation testing, Vacuum 58 (2000) 569–585.
[56] J.M. Antunes, J.V. Fernandes, N.A. Sakharova, M.C. Oliveira, L.F. Menezes, On the determination of the Young's modulus of thin films using indentation tests, International Journal of Solids and Structures 44 (2007) 8313–8334.
[57] A. Tricoteaux, G. Duarte, D. Chicot, E. Le Bourhis, E. Bemporad, J. Lesage, Depth-sensing indentation modeling for determination of Elastic modulus of thin films, Mechanics of Materials 42 (2010) 166–174.
[58] A.A. Pelegri, X. Huang, Nanoindentation on soft film/hard substrate and hard film/soft substrate material systems with finite element analysis, Composites Science and Technology 68 (2008) 147–155.
[59] A.K. Bhattacharya, W.D. Nix, Analysis of elastic and plastic deformation associated with indentation testing of thin films on substrates, International Journal of Solids and Structures 24 (1988) 1287–1298.
[60] B.J. Briscoe, Isolated contact stress deformations of polymers: the basis for interpreting polymer tribology, Tribology International 31 (1998) 121–126.
[61] C. Xiang, H.J. Sue, J. Chu, B. Coleman, Scratch behavior and material property relationship in polymers, Journal of Polymer Science, Part B: Polymer Physics 39 (2001) 47–59.
[62] W. Shen, B. Jiang, S.M. Gasworth, H. Mukamal, Study of tribological properties of coating/substrate system in micrometer and nanometer scales with a scanning probe microscope, Tribology International 34 (2001) 135–142.
[63] J. van den Brand, S. Van Gils, P.C.J. Beentjes, H. Terryn, V. Sivel, J.H.W. de Wit, Improving the adhesion between epoxy coatings and aluminium substrates, Progress in Organic Coatings 51 (2004) 339–350.
[64] P. Hu, Y. Huaming, Controlled coating of antimony-doped tin oxide nanoparticles on kaolinite particles, Applied Clay Science 48 (2010) 368–374.
[65] M. Öhman, D. Persson, C. Leygraf, In situ ATR–FTIR studies of the aluminium/polymer interface upon exposure to water and electrolyte, Progress in Organic Coatings 57 (2006) 78–88.
[66] A. Raveh, Z.K. Tsameret, E. Grossman, Surface characterization of thin layers of aluminium oxide, Surface and Coatings Technology 88 (1997) 103–111.
[67] P.R. Underhill, A.N. Rider, Hydrated oxide film growth on aluminium alloys immersed in warm water, Surface and Coatings Technology 192 (2005) 199–207.